Journal of Solid State Chemistry 183 (2010) 2101–2109

Contents lists available at ScienceDirect

Journal of Solid State Chemistry

journal homepage: www.elsevier.com/locate/jssc

Influence of Sn^{4+} and Sn^{4+}/Mg^{2+} doping on structural features and visible absorption properties of α-Fe_2O_3 hematite

M. Gaudon *, N. Pailhé, J. Majimel, A. Wattiaux, J. Abel, A. Demourgues

Institut de Chimie de la Matière Condensée de Bordeaux, UPR 9048 CNRS - Université de Bordeaux 1, 87 Avenue du Docteur Schweitzer, 33608 PESSAC Cedex, France

ARTICLE INFO

Article history:
Received 20 January 2010
Received in revised form
20 April 2010
Accepted 30 April 2010
Available online 10 June 2010

Keywords:
Hematite
Pigment
X-ray diffraction
Mössbauer spectroscopy
Visible–NIR spectroscopy

ABSTRACT

Pure, Sn-doped and Mg/Sn co-doped α-Fe_2O_3 hematite samples were synthesized by precipitation process. Fe_2O_3 is the most popular red mineral pigment which is used largely in traditional ceramics, tar and concrete. The compounds were characterized by powder X-ray diffraction (XRD), scanning transmission electronic microscopy (energy dispersive X-ray cartography), Mössbauer spectroscopy, magnetic investigations versus temperature and visible–NIR spectroscopy. Both ^{57}Fe and ^{119}Sn Mössbauer analyses combined with rietveld XRD refinements are the ideal techniques to characterize tin–iron oxides. Hence, thanks to these techniques it was shown how the synthesis temperature influences directly the grain size and the dopants concentration limit which can be incorporated into the host hematite matrix. The stabilization of these tetravalent and divalent dopants into the hematite framework leads to reduce the crystal growth and to limit the (AF) ordering due to the formation of cationic vacancies. The study of the Morin magnetic transition emphasizes this demonstration. In a second part, the influence of the dopants incorporation on the material color was investigated in order to show which key parameters allow improving the red color saturation of iron oxides. In order to improve the red color of the hematites, it was shown that the introduction of cationic vacancies—limiting the octahedral distortion thanks to the interruption of the dissymmetric metal–metal orbital coupling—is the key point. Vacancies are created by Sn^{4+}, doping for an increase of the introduced Sn^{4+} concentration; it acts to the detriment of the color saturation.

1. Introduction

α-Fe_2O_3 hematite-type mineral is an inorganic red-pigment largely used. For instance [1,2], hematite can be found as well in tattoo-inks (because of the bio-compatibility of the oxide) or city tars (because of its low cost allows its use in large quantity). Nevertheless, the mineral exhibits a red color too much dark for numerous applications such as porcelains, ceramics, tars, inks of tattooing, cosmetics, etc. Furthermore, the color strongly depends on grain size or impurities and so on the sample synthesis routes [3,4], but this dependency is until now poorly rationalized. Indeed, the α-Fe_2O_3 diffuse reflectance spectrum is built up from two main absorption edges (band-gaps) occurring in visible range about 600–700 nm, these gaps being attributed to ligand to metal $2p(O^{2-}) \rightarrow 3d(Fe^{3+})$ charge transfers as it was shown in numerous spectroscopic studies [5–10]. In our former works [11–14], it was highlighted the C_{3v} trigonal distortion of the [FeO_6] octahedra leads to an additional d orbitals splitting (crystal field theory) at the origin of this double charge transfer. One path to obtain more intense red pigments is to decrease the [FeO_6] trigonal distortion, in order to convolute the two band-gaps and thus to obtain a sharper absorption edge [4–6]. This seems possible by breaking the dissymmetric metal–metal overlapping because of the [FeO_6] octahedral chains scheduling which is constituted of face-shared dimmers separated by the empty sites. In this article, the substitution of Sn^{4+} and the co-substitution of Sn^{4+} and Mg^{2+} for Fe^{3+} ions were both attempted and compared. The study by magnetic spectroscopy of the Morin transition[TM] could be a first way leading to the investigation of the metal–metal interaction in hematite. Indeed, the magnetism of α-Fe_2O_3 exhibits a drastic spin flipping which takes place at TM. In the high-temperature (high-*T*) phase, the atomic spins lie within the (0 0 1) plane of the hexagonal structure, while they are aligned perpendicular to this plane in the low-*T* phase. The high-*T* phase is a spin-canted weak ferromagnet, while the low-*T* phase is a simple antiferromagnet without any spin canting. Of special interest from the view point of nanoscience is that the Morin transition is known to be delayed or even suppressed, i.e. the weak ferromagnetism can be preserved down to low temperatures, by decreasing the particle size [2,15–17], or by doping it [18,19]. The structural Morin transition and (AF) magnetic properties of 0.3% Sn^{4+}/Mg^{2+} co-doped α-Fe_2O_3 hematites or also SnO_2–Fe_2O_3 micro-composites were previously studied [20,21]. In the present work, the doping rate is particularly high (5–10%) thanks to the soft chemistry route

* Corresponding author.
E-mail address: gaudon@icmcb-bordeaux.cnrs.fr (M. Gaudon).

0022-4596/$ - see front matter © 2010 Elsevier Inc. All rights reserved.
doi:10.1016/j.jssc.2010.04.043

employed and such effects were never been investigated. On a fundamental point of view, the preparation of solid solutions containing Fe^{3+} and Sn^{4+} cations consists of a "school case" allowing an ideal comparative study of two techniques: X-ray diffraction (Rietveld refinement) and both ^{119}Sn or ^{57}Fe Mössbauer spectroscopies. Hence, detailed characterizations were reached (solubility limit, influence of the dopant rate on atomic positions, crystalline size information, presence of Fe^{3+} in SnO_2 impurity, etc.). Finally, a correlation between the visible–NIR absorption spectra of un-doped, doped and co-doped hematites with the structural features/chemical composition was performed in regard of our previous works devoted on such mineral. The key parameters to obtain the most reddish color in iron hematite were here clearly isolated.

2. Experimental details

2.1. Synthesis process

Sn^{4+} and Sn^{4+}/Mg^{2+} doped Fe_2O_3 pigments were synthesized by a co-precipitation process in basic medium. 7.2 M NH_4OH solution was added into a Fe^{3+} 0.5 M (pH 1) aqueous solution of iron nitrate ($Fe(NO_3)_3 \cdot 9H_2O$), tin chloride ($SnCl_4$) and magnesium chloride ($MgCl_2$) in order to precipitate metal ions on a mixed amorphous precipitate which can be consider as an oxy-hydroxide form: Sn or Mg–Sn-doped-Fe(O_y-OH_z). According to the iron Pourbaix diagram and literature studies [22–24], solid iron hydroxide, oxide or aqueous-oxide can be precipitated depending on oxidizing–reducing conditions in a large pH range into aqueous solutions, from 4.5 to 10. The chosen working pH is 9.5. The brown precipitate was dried overnight at 100 °C. Then, in order to obtain the final Sn or Sn/Mg-doped α-Fe_2O_3 oxide, a thermal treatment at various temperatures (400, 600 and 800 °C) for 6 h under air was performed with a heating/cooling rate of 1 °C min^{-1}.

2.2. X-ray powder diffraction

A Philips PW 1820 apparatus equipped with a Cu($K\alpha_1/K\alpha_2$) source ($\lambda_{average}=1.5424$ Å) was used to evaluate crystalline structure of all synthesized compounds. Diffraction patterns were collected with a 2θ step of 0.02° with a counting time of 10 s per step. While the full width height media (FWHM) of the diffractions peak is large enough, the average crystallite size of the sample was evaluated; the determination of the anisotropic grain size for these hematite-type phases was developed in a previous paper [13]. For more advanced structural investigations, X-ray diffraction (XRD) measurements were carried out on a PANalytical X'PERT PRO diffractometer equipped with a X-celerator detector, using Co($K\alpha_1/K\alpha_2$) radiation ($\lambda_{average}=1.7909$ Å) to limit the fluorescence of Fe. XRD data were recorded with a 2θ step=0.017°. Diffractograms have been refined with Rietveld refinement method [25], using FULLPROF® program package. Unit cell parameters, anisotropic shape of the crystallites, atomic positions, occupancies and Debye–Waller factors have been refined.

2.3. Mössbauer spectroscopy

In order to evaluate Fe^{3+} local environments and magnetic ordering of the studied ferrite compounds, ^{119}Sn Mössbauer measurements were performed at 293 and 4 K while ^{57}Fe measurements were performed at 293 K. Both analyses are in transmission mode and were led using a conventional constant acceleration spectrometer (HALDER) with rhodium matrix source. As the samples contain between 5 and 8 mg natural iron per cm^3, the line broadening due to thickness of samples can be neglected. The spectra refinement was performed in two steps. Firstly, the fitting of Mössbauer patterns as a series of Lorentzian profile peaks allowed the calculation of position (δ), amplitude and width (Γ) of each peak: thus, experimental hyperfine parameters were determined for the various iron sites. Secondly, spectra analysis was made in terms of quadripolar splitting distribution $P(\Delta)$ and/or hyperfine field distribution $P(H)$ using the Hesse and Rubartsch method [26]; Γ and δ were fixed at values determined in the first refinement. This method, which was used because of the line broadening notably observed, leads to a peak shape different from a Lorentzian profile which is characteristic of disordered compounds with a sites distribution.

2.4. Magnetic measurements

The magnetic susceptibilities measurements versus temperature were performed on an automatic susceptometer DSM-8 equipped with a liquid nitrogen cryostat and an electromagnet Brucker BE-15 which works at temperatures ranging from 77 up to 400 K.

2.5. Scanning transmission electronic microscopy

Scanning Transmission Electronic Microscopy (STEM) experiments were performed on JEOL 2200FS equipment with a Schottky field-emission gun, operating at 200 kV. STEM samples were prepared by dispersing few milligrams of powder in ethanol. The solution was then dipped 10 min into an ultrasonic bath in order to disagglomerate and disperse powder particles. One drop of the solution was finally deposited on a Formvar/carbon copper grid. Chemical mappings were performed using a JEOL EDX system (50 mm2 Si(Li) detector) with a probe size of about 0.8 nm, which is a good compromise between signal intensity and spatial resolution.

2.6. Diffuse reflectance measurements

The visible–NIR spectroscopic analyses were carried out in Diffuse Reflectance mode on a VARIAN CARY 5000 spectrophotometer equipped with an integrating sphere coated with polytetrafluoroethylene (PTFE). Measurements were performed for wavelengths varying from 200 nm up to 2000 nm. HALON was used as white reference. Only the UV–visible wavelength range is discussed in this paper.

A mathematic treatment of the obtained spectra allowed the determination of the La^*b^* space colorimetric parameters. The first step of the treatment consists to obtain the *XYZ* tri-stimulus values (defined by the CIE, 1964) from the integration (on the visible range, i.e. from $\lambda=380$ nm up to 780 nm) of the product of $x(\lambda)$, $y(\lambda)$ or $z(\lambda)$ functions (CIE—1964) with the diffuse reflectance spectra function: $X=\int x(\lambda)\,R(\lambda)\,d\lambda$. Then, the transfer equations defined by the CIE, 1976, from XYZ space to the La^*b^* space, were used in order to obtain, La^*b^* chromatic parameters (L: luminosity, a^*: green to red axis and b^*: yellow to blue axis coefficients). The illuminant used was the D65 (daylight) with a 10° orientation.

3. Results and discussion

Even if, a complete set of modified hematite samples was synthesized with numerous doping and co-doping rates (5, 10 and 15 mol% for the dopants: Sn/Mg or Sn) and for different

calcination temperatures (400–600–800–1400 °C), in order to remain the clearest as possible, only results obtained on the 5 mol% Sn-doped and 5/5 mol% Sn/Mg co-doped samples obtained at 400 and 800 °C annealing temperatures are here reported. Actually, the other data appear redundant with these first ones. However, it indicates the reproducibility of the reported results.

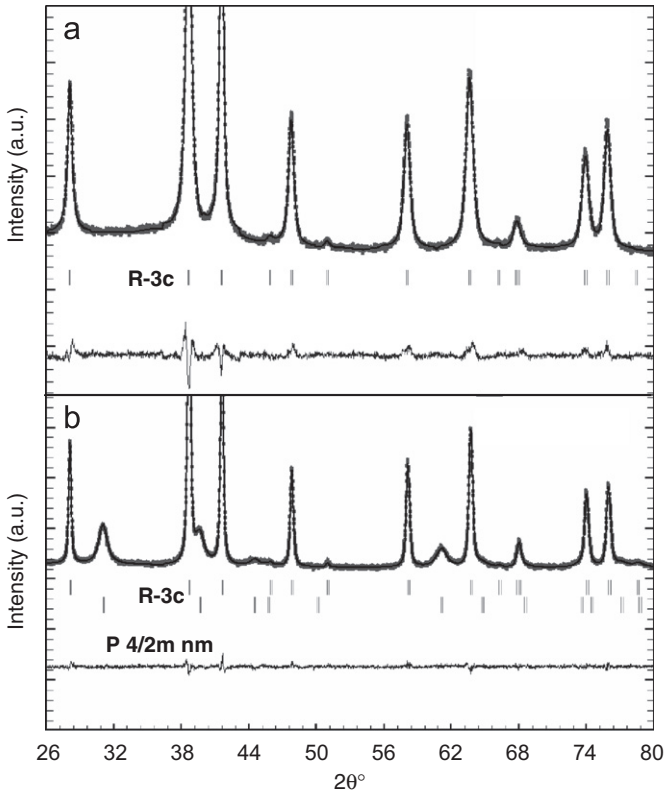

Fig. 1. X-ray patterns, Bragg positions and difference of the performed refinement for the 5 mol% Sn-doped Fe_2O_3 annealed at 400 °C (a) and 800 °C (b).

3.1. 5 mol% Sn-doped Fe_2O_3

From X-ray diffraction analyses, after calcination at 400 °C (Fig. 1a), the Sn-doped hematite exhibits only diffraction peaks which can be indexed in the corundum network: all diffraction peaks correspond to the standard $R-3c$ space group. However, after calcination at 800 °C (Fig. 1b), the presence of a well crystallized SnO_2-type phase ($P4/2mnm$ space group) is clearly detected besides the hematite main phase. The Rietveld refinement results of the hematite phase which are reported in Table 1 clearly show the growing of the crystallites between 400 and 800 °C. The determination of the anisotropic grain size for these hematite-type phases was developed in a previous paper [6]. Furthermore, the x oxygen anion (x_O) position is strongly affected by the annealing temperature. Indeed, x_O position is about 0.312 for the 400 °C-annealed crystallites, whereas for the 800 °C-annealed crystallites, x_O position is then decreased until literature standard value of 0.307 [27–30]. Other refined parameters (z_{Fe}, B_{iso}) do no vary significantly between $T=400$ and 800 °C (annealing temperatures). Moreover the reliability factors remain quite constant.

Results from ^{57}Fe Mössbauer studies are reported in Fig. 2. Firstly, for comparison, the signal of an un-doped Fe_2O_3 hematite sample synthesized under same conditions is reported. For pure Fe_2O_3, only characteristic anti-ferromagnetic sextuplets can be seen for both compounds obtained after calcination at 400 and 800 °C. For doped compounds, a quadripolar doublet, characteristic of paramagnetic or "super-paramagnetic" Fe^{3+} ions is observable for the compound calcined at 400 °C. The spectrum of the 800 °C Sn-doped sample do not differ from

Table 1
Rietveld refinements results of the Sn-doped and Mg/Sn co-doped compounds.

Sn–Fe_2O_3—400 °C					
a=**5.0442**(5) Å	R_p=1.78%−R_{wp}=2.24%				
c=**13.785**(1) Å	R_{Bragg}=7.00%				
Atom	**Site**	***x***	***y***	***z***	**Biso**
Fe/Sn	12c	0	0	**0.3541(5)**	0.3(1)
O	18e	**0.312(2)**	0	¼	0.7(1)
Grain sizes (1 0 0)=225 nm/(0 0 1): 120 nm					
Sn–Fe_2O_3—800 °C					
a=**5.0510**(3) Å	R_p=2.08%−R_{wp}=2.62%				
c=**13.779**(1) Å	R_{Bragg}=4.21%				
Atom	**Site**	***x***	***y***	***z***	**Biso**
Fe/Sn	12c	0	0	**0.3551**(2)	0.4(1)
O	18e	**0.307**(1)	0	¼	0.2(1)
Grain sizes too large to be solved					
Sn/Mg–Fe_2O_3—400 °C					
Amorphous compound					
Sn/Mg–Fe_2O_3—800 °C					
a=**5.0543**(4) Å	R_p=2.14%−R_{wp}=2.75%				
c=**13.779**(1) Å	R_{Bragg}=4.44%				
Atom	**Site**	***x***	***y***	***z***	**Biso**
Fe/Sn/Mg	12c	0	0	**0.3549**(2)	0.3(1)
O	18e	**0.307**(1)	0	¼	0.4(1)
Grain sizes too large to be solved					

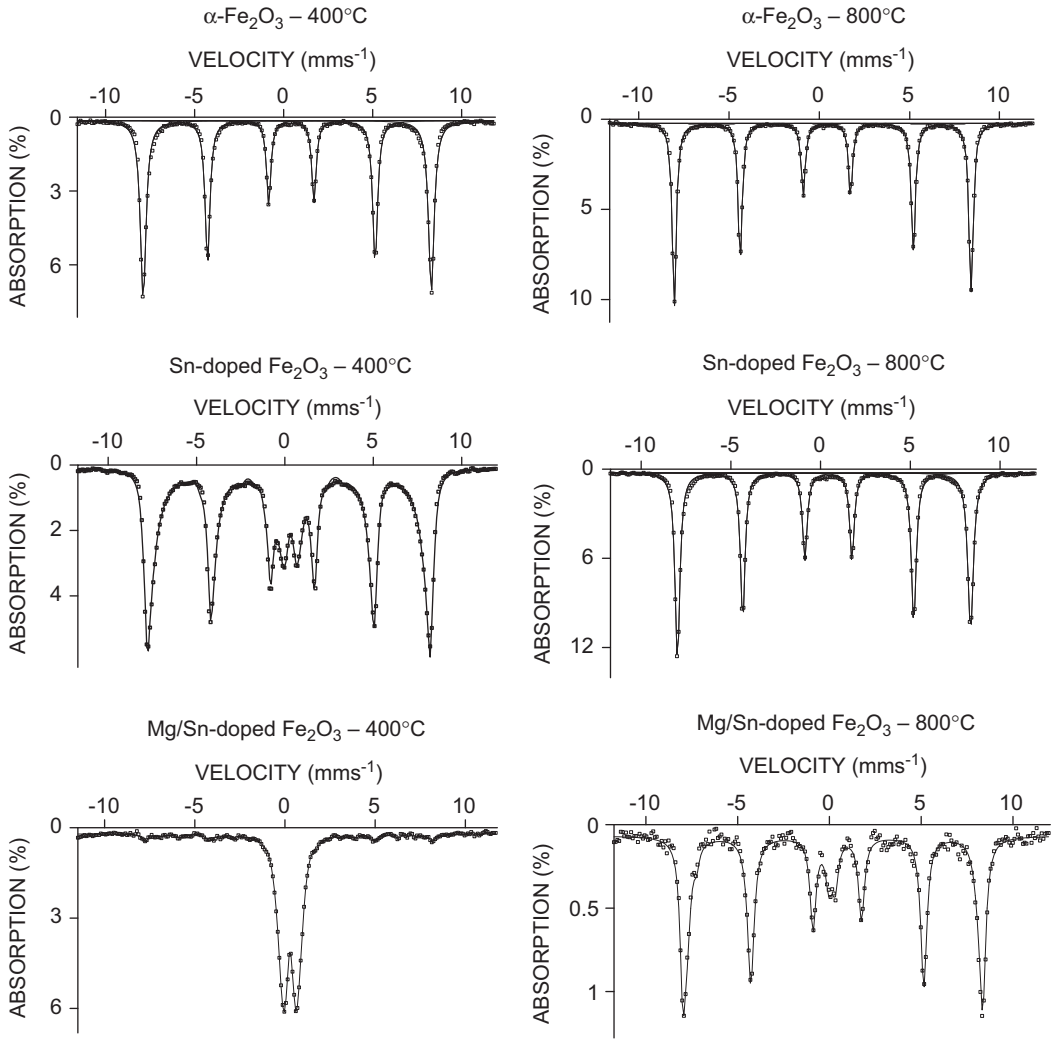

Fig. 2. ^{57}Fe (298 K) Mössbauer spectra of pure, Sn-doped and Sn/Mg-doped Fe_2O_3.

un-doped reference one. From ^{119}Sn Mössbauer studies performed at room temperature, reported in Fig. 3, a non-negligible anti-ferromagnetic field is clearly transferred from the Fe^{3+} towards Sn^{4+} cations for the 400 °C calcined sample whereas no trace of transferred field on tin is detectable after calcination at 800 °C, as it was previously shown in the literature [31]. Furthermore, another set of analyses performed at 4 K shows a complete disappearance of the paramagnetic contribution for the spectrum corresponding to Sn-doped sample annealed at 400 °C, i.e. the Sn^{4+} ions exhibit spin polarization.

The magnetic behavior of the Sn-doped hematite obtained after calcination at 400 °C (curve c, Fig. 4), after calcination at 800 °C (curve b, Fig. 4) in comparison with a pure Fe_2O_3 (curve a) shows significant changes: (i) in both doping cases, decreases of the Morin transition amplitude and temperature compared to the un-doped sample; (ii) more important effect for the sample annealed at 400 °C than for the sample annealed at 800 °C. As already established [17,18], the Morin transition in hematite, which can be described as a brutal reinforcement of the perfection of the AF ordering while the temperature decreases below the Morin transition, is very sensitive to cation substitution. Indeed, while the insertion of cationic impurities "breaks" the Fe–Fe metal to metal magnetic interaction, a decrease of the Morin transition amplitude is expected. Besides the Sn-doped samples annealed at 800 °C exhibiting Morin transition at about 210 K (250 K for un-doped Fe_2O_3), the magnetic curve of the doped sample annealed at only 400 °C shows no transition. Hence, this investigation shows clearly that the Sn^{4+} ions incorporated at 400 °C partially diffuse out of the hematite during the heating from 400 to 800 °C. It is an indirect proof of the sample thermal history influence on the Sn^{4+} solubility limit in hematite. The direct proof was obtained by transmission electron microscopy coupled with ultra-local EDX analyses performed on the two doped samples annealed at different temperature. As shown in Fig. 5, were the 400 °C sample (Fig. 5a) is compared to the 800 °C-one (Fig. 5b), one can see that the homogeneity of the distribution of Sn^{4+} achieved at 400 °C is significantly damaged after an annealing at 800 °C, synthesis conditions for which cluster of nearly pure tin oxides can be easily visualized.

Hence, one can conclude thanks to the whole analyses that a pure metastable phase (Sn^{4+} doped Fe_2O_3) is obtained after calcination at 400 °C, this latter decomposing while grain growths during the calcination of the sample at higher temperature. This decomposition versus synthesis temperature can be notably followed by the evolution of the oxygen atomic position which tends to show that Sn^{4+} ions are rejected from the hematite grains. Indeed, the x_O evolution versus annealing temperature shows that cation octahedral sites are more and more distorted with increasing the temperature (for an anionic cage with a ideal Oh geometry point group, the x_O position should be 0.333). This

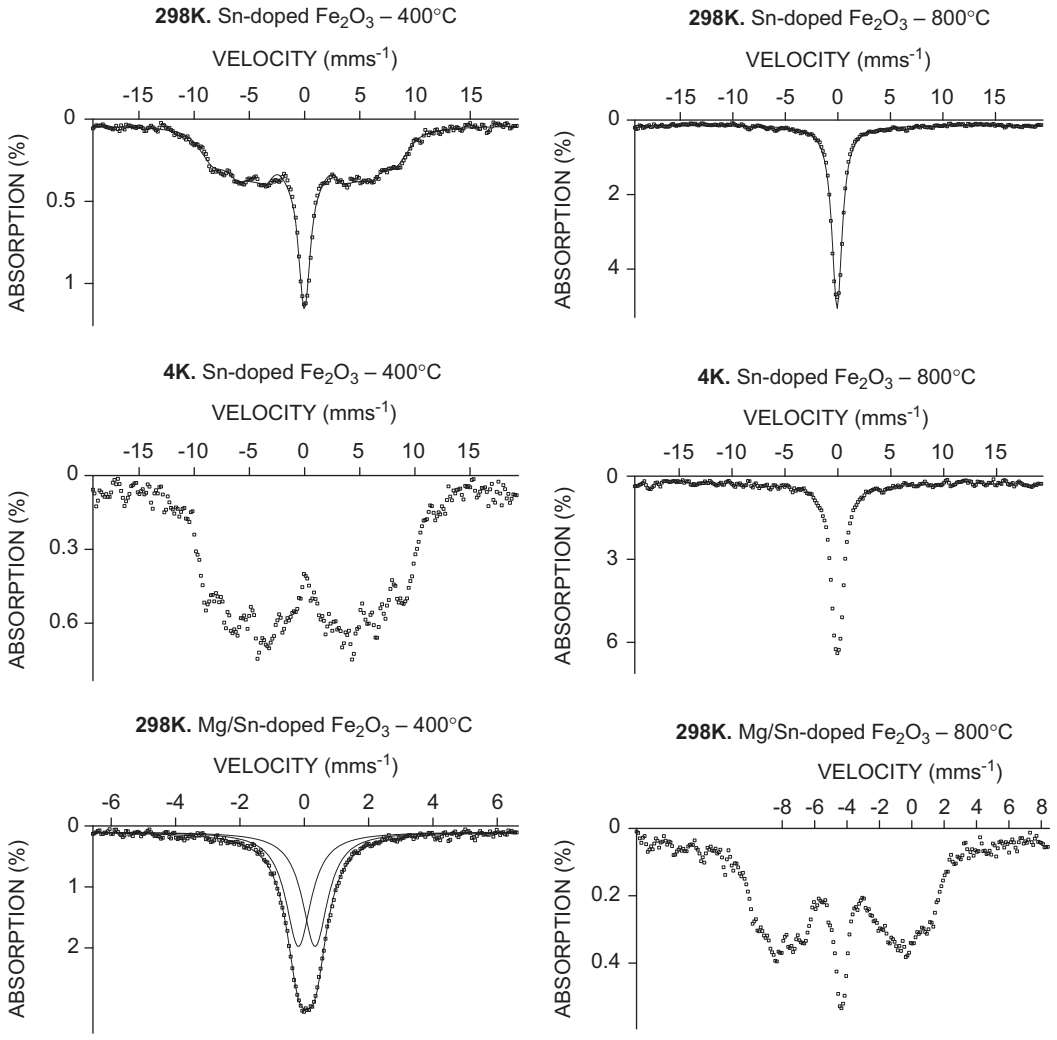

Fig. 3. ^{119}Sn (298 or 4 K) Mössbauer spectra of pure, Sn-doped and Sn/Mg-doped Fe_2O_3.

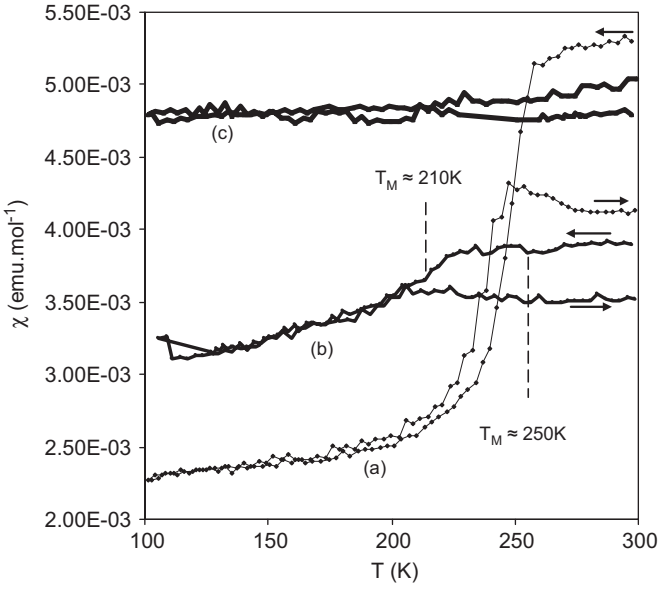

Fig. 4. Magnetic measurements inside 100–300 K range of (a) Fe_2O_3 at 800 °C, (b) 5 mol% Sn-doped Fe_2O_3 annealed at 800 °C, (c) 5 mol% Sn-doped Fe_2O_3 annealed at 400 °C.

shows that, with annealing, less and less Sn^{4+} ions are incorporated in the host matrix; the Sn^{4+} ions substituted for Fe^{3+} or the associated vacancies created in order to compensate the electroneutrality perturbing the face-sharing octahedral network at the origin of the site distortion. The Sn demixing out from the hematite matrix during the post-annealing can be explained by our liquid route which allows the preparation of highly divided oxide powder when a low annealing temperature is used. Then, the metastable phase obtained after the 400 °C annealing seems stabilized because of the large specific surface linked to small particle size. Furthermore, for the 400 °C sample, the hypothesis of an amorphous tin-rich phase besides the crystalline doped hematite can be eliminated thanks to ^{119}Sn Mössbauer studies. The spin polarization, partial at room temperature but total at 4 K seems to show that the whole of tin ions is incorporated inside hematite structure. This is clearly shown for the 400 °C annealed compound, since Sn^{4+} ions exhibit a spin polarization which can only be transferred by the Fe^{3+} ions of the hematite network. Consequently, super-paramagnetism observed with ^{57}Fe Mössbauer technique for the 400 °C annealed doped sample is without any doubt not only linked to the small crystallite size but also to the incorporation of Sn^{4+} ion. Finally, the disappearance of the transferred anti-ferromagnetic field from Fe^{3+} to Sn^{4+} ions for the 800 °C annealed sample brings to the fore that the SnO_2 second phase formation during the annealing step comes from the

firstly incorporated Sn^{4+} ions which diffuse out of the hematite crystallites.

3.2. 5-5 mol% Sn/Mg co-doped Fe_2O_3 and comparison with the previous sample

After annealing at 400 °C, the obtained powder remains amorphous, at least non-visible from X-ray diffraction technique. However, the co-doped compound annealed at 800 °C is well crystallized. In comparison with the Sn-doped compound obtained for the same annealing temperature, significantly less SnO_2-type phase is detected on X-ray diffraction patterns as it can be seen comparing Figs. 1b and 6.

^{119}Sn Mössbauer analyses (Fig. 4, bottom ones) show that conversely to the Sn-doped compound, an anti-ferromagnetic contribution remains persistent after 800 °C annealing. Moreover, it can be noticed that the ^{57}Fe Mössbauer analyses (Fig. 3, bottom ones) is a powerful technique to follow hematite crystallization; indeed, no AF ordering is observed until the hematite network organization is achieved, i.e. for the 400 °C-annealed co-doped compound. Consequently, Mössbauer spectrum exhibits for this sample only a quadripolar doublet which is characteristic of the absence of a magnetic ordering. Finally, it has to be noticed the

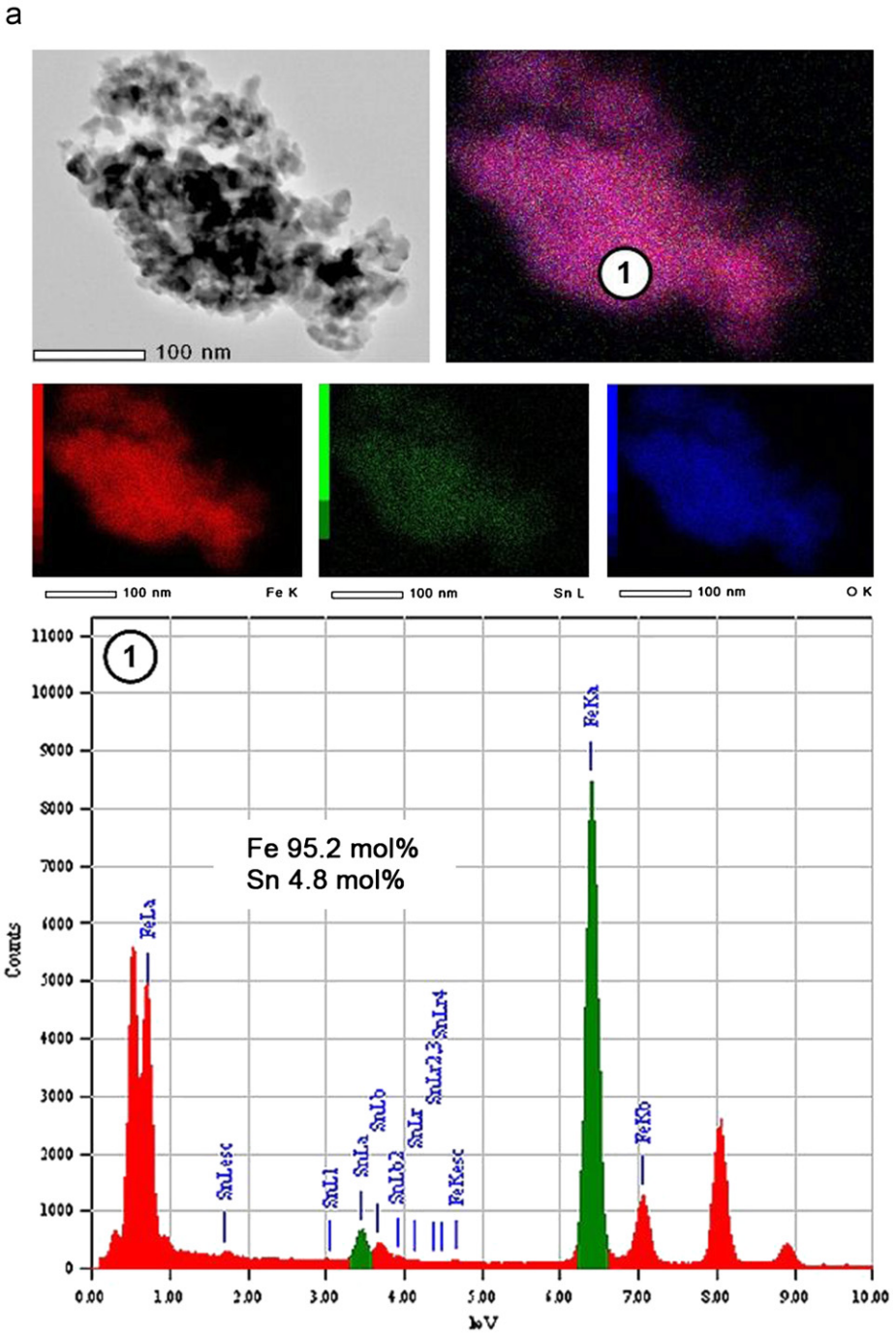

Fig. 5. STEM sample images, corresponding elemental cartographies and EDX spectrum on (a) 5 mol% Sn-doped Fe_2O_3 annealed at 400 °C, (b) 5 mol% Sn-doped Fe_2O_3 annealed at 800 °C. In the RGB images (upper-right) every pixel has three channels (red–green–blue) associated to the three elemental maps assigned respectively to the Fe, Sn, and O elements. (For interpretation of the references to color in this figure legend, the reader is referred to the web version of this article.)

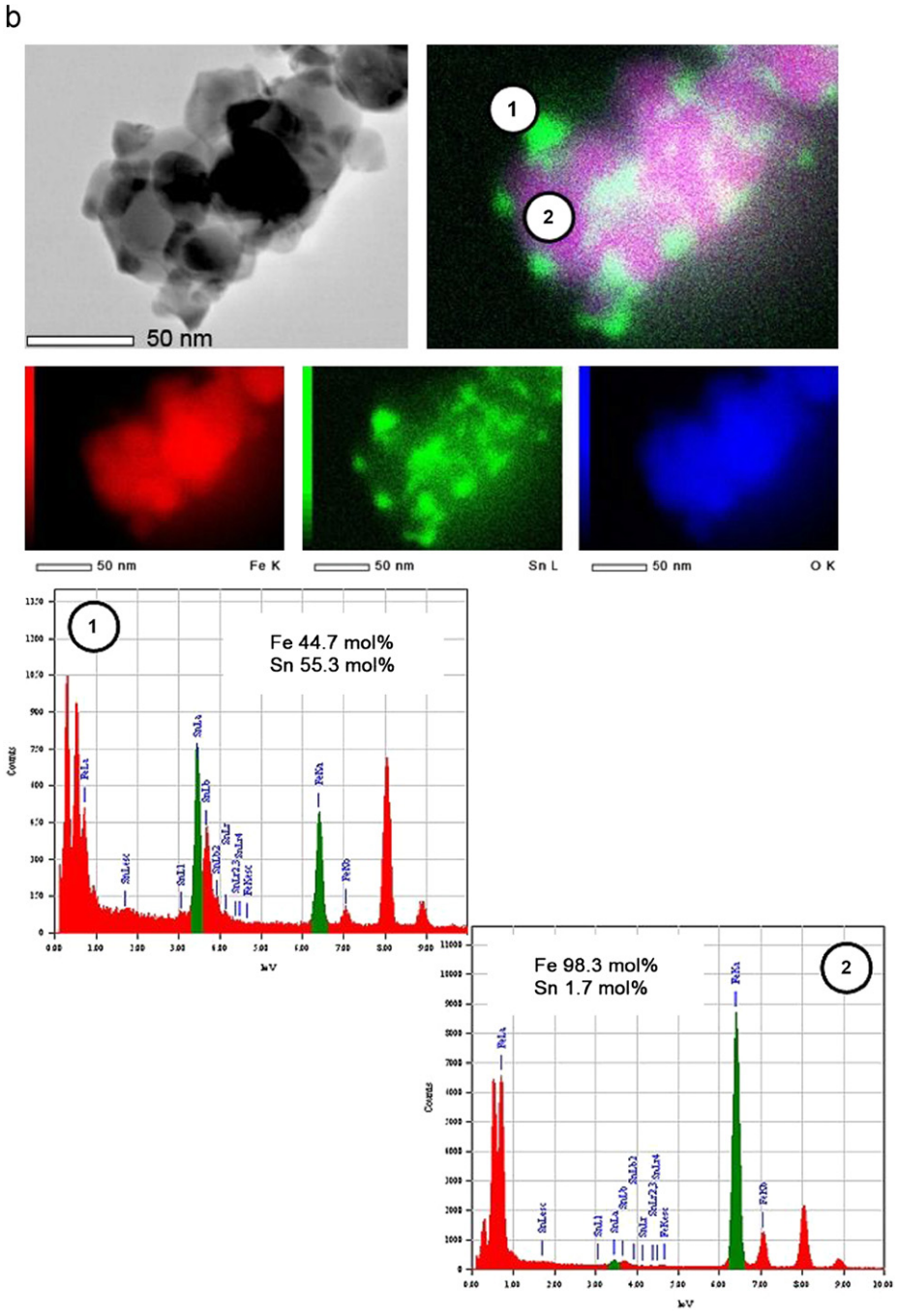

Fig. 5. (*Continued*)

occurrence besides the AF sextuplets of a persistent iron paramagnetic contribution (quadripolar doublet) for the 800 °C-annealed co-doped compound.

The Mg/Sn co-doping, in comparison with the single Sn doping, strongly delays the hematite crystallization; the synthesized oxide remaining amorphous after a 400 °C heating. The difficulty to incorporate magnesium into hematite structure can probably be linked to the origin of the crystallization delay. However, from X-ray patterns, it clearly appears that the co-doping allows incorporating, inside hematite host matrix, Sn^{4+} ions in larger quantity than the single Sn doping, comparing similar annealing temperatures. The pattern refinement results do not bring any supplementary information: the refined x_O position for instance, which is characteristic of the octahedral sites distortion, does not differ significantly from un-doped hematite. Mössbauer analyses confirm the observations made from X-ray patterns, i.e. the large improvement of the solubility limit of Sn^{4+} in hematite structure for comparable synthesis temperature. In this way, the paramagnetic contribution observed from ^{57}Fe Mössbauer spectrum for the 800 °C co-doped compound is consistent with a limited spatial extension of the magnetic ordering inside the hematite network; the reduced spatial extension being caused by the presence of Sn^{4+} and Mg^{2+} specific defects. Moreover, the improvement reached from the Mg^{2+} ions besides Sn^{4+} incorporation in Fe_2O_3 is shown by the AF transferred field detected by ^{119}Sn spectroscopy on the 800 °C co-doped compound.

The studies on the co-doped sample show that the respect of the compound electroneutrality allows single phase decomposition delay versus annealing temperature. Then, one can assume that the first limitation of the incorporation of Sn^{4+} inside hematite is the subsequent creation of compensation cationic vacancies. Indeed, Sn^{4+} seems intrinsically well supported by the host network since for Mg/Sn co-doped hematite, Sn^{4+} is detected in hematite network even after high annealing temperatures. It can be added that effectively, a cation vacancy creates more disequilibrium within crystallographic network than the substitution of a cation for another one, as well from a steric or an electronic point of views. This appears especially obvious in our case for which host and doping elements get proximal charges and roughly the same ionic sizes: 0.690 Å for Sn^{4+}, 0.720 Å for Mg^{2+} instead of 0.645 Å for Fe^{3+} (ionic radii for 6-fold coordination from Shannon and Prewitt tables).

3.3. Application: diffuse reflectance properties

In our previous papers [4,6], it has been shown that the reddish color of hematite is browned by a double gap in visible range caused by the octahedral iron sites deformation (C_{3v} distortion). The starting point was that the face-sharing chains of the iron octahedral sites which could be perturbed by as well Sn^{4+} or associated cationic vacancies, leading thus to less distorted octahedral sites. Hence, one can think that Sn doping could allow the preparation of more red pigment (with a higher a^* colorimetric parameter, representative of the color position on the green–red axis).

The La^*b^* trichromatic parameters reported inside Table 2 underline that the Sn single doping is largely more efficient than the Mg/Sn co-doping for pigment application, the a^* parameter, related to the red saturation, being notably the highest for the 400 °C single Sn-doped compound. Moreover, the colorimetric values of the 400 °C-Mg/Sn co-doped compound differ strongly from the others probably because this compound is amorphous and cannot be compared to the others. For the 800 °C-Mg/Sn co-doped sample, X-ray diffraction and Mössbauer analyses show that the Sn^{4+} inserted rate is superior to the Sn^{4+} incorporated one for a single doping. Nevertheless, the colorimetric parameters are optimal for this latter, thanks to the cationic vacancies allowing a relaxation of the octahedral site distortion. A last study reported in Fig. 7, proposes a comparison of the diffuse reflectance curves of commercial hematite (synthesized at 1400 °C), 400 °C-annealed Fe_2O_3 and 400 °C-annealed Sn-doped hematite. This investigation confirms (i) while the two absorption edges are more and more convoluted, the a^* is more and more positive, (ii) the grain size decrease and/or the introduction of Sn^{4+} inside the host matrix leads, via the associated cationic vacancies creation, to an octahedral site distortion relaxation and can be so considered at the origin of a more convoluted double gap. Indeed, the high energy bandgap (low wavelengths) is significantly shifted through low energy while Sn doping or grain size decrease whereas the low energy gap is only very slightly affected: the first one is calculated from inflexion point at 560, 580 and 600 nm for a commercial hematite, nano-size hematite and nano-size Sn-doped hematite, respectively, the second one only vary between 705 and 711 nm. Hence, even if the effects are limited, the non-isovalent substitution of Fe^{3+} (here for Sn^{4+}) inside hematite host matrix is really a key parameter in order to improve the red color of hematite pigment.

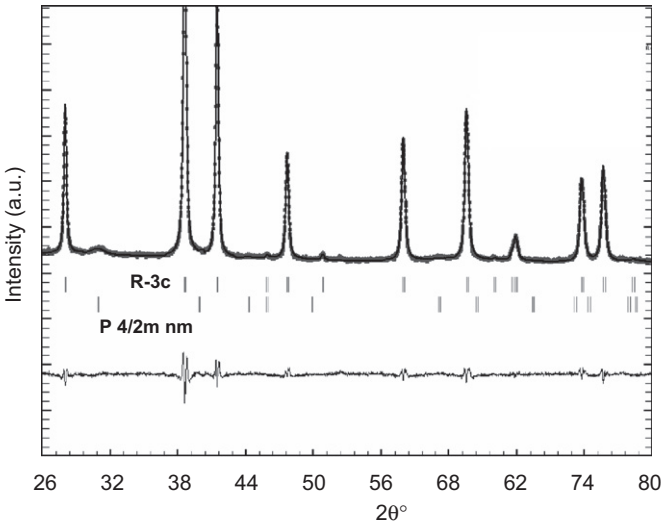

Fig. 6. X-ray patterns, Bragg positions and difference of the performed refinement for the 5 mol% Sn/Mg-doped Fe_2O_3 annealed at 800 °C.

Table 2
La^*b^* colorimetric parameters of the various synthesized compounds.

Sample	L^*	a^*	b^*
Fe_2O_3—400 °C	30.4	21.4	19.5
Fe_2O_3—800 °C	35.0	18.7	17.5
Sn–Fe_2O_3—400 °C	29.5	**23.2**	22.5
Sn–Fe_2O_3—800 °C	35.1	19.8	20.4
Mg/Sn–Fe_2O_3—400 °C	*31.6*	*12.7*	*14.6*
Mg/Sn–Fe_2O_3—800 °C	34.8	19.8	21.3

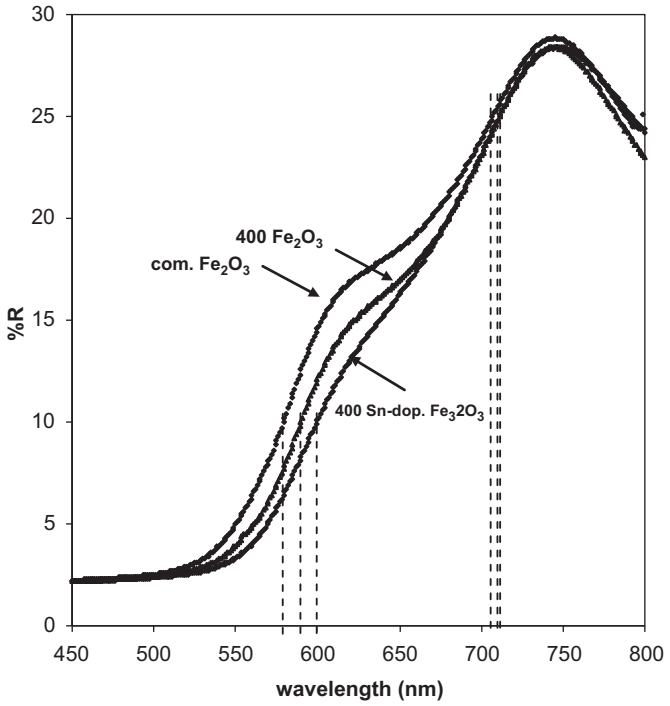

Fig. 7. Diffuse reflectance curves in the visible region of various hematite samples.

4. Conclusion

In this work, the combination of X-ray diffraction, ^{119}Sn and ^{57}Fe Mössbauer analyses and magnetic measurements were used to study of Sn-doped and Mg/Sn co-doped hematites synthesized via "*chimie douce*" process. The chosen investigation techniques allowed

underlining without any doubt that Sn^{4+} coupled or not with Mg^{2+} can be introduced in small fraction in hematite phase forming a "metastable compound". Indeed, versus increasing temperatures, it is here shown that the incorporated Sn^{4+} ions partially leave out the hematite network. This demixion is clear on the basis of Mössbauer spectroscopy, XRD analyses and STEM–EDX measurements. The Mg^{2+} co-substitution, thanks to electronic and steric constrains relaxation partially prevents the Sn^{4+} ions demixion. The doped compounds obtained at low temperature exhibit a more reddish hue because the doping allows octahedral distortion relaxation by breaking the octahedral chains organization. Even if the pigment color enhancement is not really important, this study confirms the key parameter allowing tuning the red color of iron-based pigments: the iron octahedral site distortion.

Iron-based oxides are ones of the rare non-toxic mineral matrixes. On the basis of this study, the limitation of FeO_6 octahedral sites distortion by using various counter-ions as well as the design of new frameworks where Fe–O bond distances are regular will lead to obtain more and more reddish mineral powder, a very important target in the pigment industry.

References

[1] A.L. Peter (Ed.), Pigment Handbook, John Wiley & Sons, New York, USA, 1987.
[2] R.M. Cornell, U. Schwertman, The Iron Oxides: Properties, Reactions, Occurrence, and Uses, Weinheim, New York, VCH, 1996, pp. 1–25.
[3] H. Katsuki, S. Komarneni, J. Am. Ceram. Soc. 86 (1) (2003) 183–185.
[4] L. Dengxin, G. Guolong, M. Fanling, J. Chong, J. Hazard. Mater. 155 (1–2) (2008) 369–377.
[5] K.J. Sreeram, R. Indumathy, A. Rajaram, B.U. Nair, T. Ramasami, Mater. Res. Bull. 41 (10) (2006) 1875–1881.
[6] M. Elias, C. Chartier, G. Prévot, H. Garay, C. Vignaud, Material Science Eng. B 127 (2006) 70–80.
[7] C.S. Kosmas, D.P. Franzmeier, D.G. Schulz, Clays Clay Miner. 34 (6) (1986) 625–634.
[8] G.R. Rossman, in: M.D. Dyar, C. McCammon, M.W. Schaefer (Eds.), The Geochemical Society, Special Publication No. 5, 1996, pp. 23–27.
[9] D.M. Shermann, T.D. Waite, Am. Miner. 70 (1985) 1262–1269.
[10] J. Torrent, V. Barron, Clays Clay Miner. 51 (3) (2003) 309–317.
[11] N. Pailhé, A. Wattiaux, M. Gaudon, A. Demourgues, J. Solid State Chem. 181 (10) (2008) 2697–2704.
[12] N. Pailhé, A. Wattiaux, M. Gaudon, A. Demourgues, J. Solid State Chem. 181 (5) (2008) 1040–1047.
[13] N. Pailhé, S. Pechev, J. Majimel, P. Graverau, M. Gaudon, A. Demourgues, J. Phys. Chem. C 112 (49) (2008) 19217–19223.
[14] M. Gaudon, N. Pailhé, A. Wattiaux, A. Demourgues, Mater. Res. Bull. 44 (3) (2009) 479–484.
[15] Y. Bando, M. Kiyama, N. Yamamoto, T. Takada, T. Shinjo, H. Takaki, J. Phys. Soc. Japan 20 (1965) 2086.
[16] R.E. Vandenberghe, C.A. Barrero, C.A. Da Costa, E. Van San, E. De Grave, Hyperfine Interact. 126 (2000) 247–259.
[17] R.E. Vandenberghe, E. De Grave, C. Landuydt, L.H. Bowen, Hyperfine Interact. 53 (1990) 175.
[18] C.A. Barrero, J. Arpe, E. Sileo, L.C. Sa´nchez, R. Zysler, C. Saragovi, Physica B: Condens. Matter 354 (2004) 27–34.
[19] O. Helgason, F.J. Berry, T. Moyo, X. Ren, AIP Conf. Proc. 765 (2005) 206–210.
[20] P.B. Fabritchnyi, E.V. Lamykin, A.M. Babechkin, A.N. Nesmeianov, Sol. State. Commun. 11 (1972) 343–348.
[21] N. Hayashi, S. Muranaka, S. Yamamoto, M. Takano, D.-F. Zhang, L.-D. Sun, C.-H. Yan, J. Solid State Chem. 181 (12) (2008) 3283–3286.
[22] M. Loan, G.M. Parkinson, W.R. Richmond, Am. Mineralog. 90 (2005) 258–261.
[23] Y. Cudennec, A. Lecerf, J. Solid State Chem. 179 (3) (2006) 716–722.
[24] M. Pourbaix, Atlas d'équilibres électrochimiques à 25 °C, Gauthier-Villars, Paris, France, 1963.
[25] H.M. Rietveld, Acta Cryst. 22 (1967) 151–152;
H.M. Rietveld, J. Appl. Cryst. 2 (1969) 65–71.
[26] J. Hesse, A. Rubartsch, J. Phys. E. Sci. Instrum. 7 (1974) 526.
[27] K. Kelm, W. Mader, Z. Anorg. Allg. Chem. 631 (2005) 2383–2389.
[28] H. Sawada, Mat. Res. Bull. 31 (2) (1996) 141–146.
[29] E.N. Maslen, V.A. Strel'tsov, N.R. Strel'tsova, N. Ishizawa, Acta Cryst. B 50 (1994) 435–441.
[30] E. Wolska, U. Schwertmann, Z. Krist. 189 (1989) 223–237.
[31] V.V. Kovalenko, M.N. Rumyantseva, F.B. Fabritchnyi, A.M. Gaskov, Mendeleev Commun. 14 (4) (2004) 140–141.